Impact of modified turbulent diffusion of PM$_{2.5}$ aerosol in WRF-Chem simulations in Eastern China

Wenxing Jia[1,2], Xiaoye Zhang[2,3*]

[1]Key Laboratory for Aerosol-Cloud-Precipitation of China Meteorological Administration, Nanjing University of Information Science & Technology, Nanjing, 210044, China

[2]Key Laboratory of Atmospheric Chemistry of CMA, Chinese Academy of Meteorological Sciences, Beijing, 100081, China

[3]Center for Excellence in Regional Atmospheric Environment, IUE, Chinese Academy of Sciences, Xiamen, 361021, China

Correspondence to: X. Zhang (xiaoye@cma.gov.cn)

Abstract

Correct description of the boundary layer mixing process of particle is an important prerequisite for understanding the formation mechanism of pollutants, especially during heavy pollution episodes. Turbulent vertical mixing determines the distribution of momentum, heat, water vapor and pollutants within the planetary boundary layer (PBL). However, turbulent mixing process of particles is usually denoted by turbulent diffusion of heat in the WRF-Chem model, which is questionable. Using mixing-length theory, the turbulent diffusion relationship of particle is established, embedded into the WRF-Chem and verified based on long-term simulations from 2013 to 2017. The new turbulent diffusion coefficient is used to represent the turbulent mixing process of pollutants separately, and not to deteriorate the simulation results of meteorological parameters. The new turbulent diffusion improved the simulation of pollutant concentration to varying degrees, and the simulated results of PM$_{2.5}$ concentration were

improved by 8.3% (2013), 17% (2014), 11% (2015) and 11.7% (2017) in Eastern China, respectively. Furthermore, the pollutant concentration is expected to increase due to the reduction of turbulent diffusion in mountainous areas, but the pollutant concentration did not change as expected. Therefore, under the influence of complex topography, the turbulent diffusion process is insensitive to the simulation of the pollutant concentration. For mountainous area, the evolution of pollutants is more susceptible to advection transport, due to the simulation of obvious wind speed gradient and pollutant concentration gradient. In addition to the $PM_{2.5}$ concentration, CO as a primary pollutant, its concentration has also been improved, which shows that the turbulent diffusion process is extremely critical for variation of the various aerosol pollutants. Additional joint research on other processes (e.g., dry deposition, chemical and emission processes) may be necessary to promote the development of the model in the future.

1 Introduction

Along with the intensive urbanization and tremendous economic development, numerous incidents of aerosol pollution have frequently occurred in China (An et al., 2019; X. Zhang et al., 2019). Aerosol pollution, characterized by $PM_{2.5}$, occurs primarily within the planetary boundary layer (PBL). The horizontal transportation and vertical diffusion of pollutants are obviously affected by the PBL mixing process, associated with intricate turbulent eddies (Ren et al., 2018; Wang et al., 2018; Du et al., 2020). Turbulent diffusion, as a vital process, controls the exchange of momentum, heat, water vapor and pollutants through turbulent eddies within the PBL (Stull, 1988).

Moreover, PBL height (PBLH) directly determines the effective air volume of pollutant diffusion and atmospheric environmental capacity. With the continuous development of technology, there are numerous means (e.g., radiosonde, tethered balloon, meteorological tower, aircraft, ground-based remote sensing and space-based remote sensing) and methods (e.g., based on surface fluxes, Richardson number and others

diagnostic methods) to determine the PBLH, of course, the results are also different (Zhang et al., 2020). It is worth noting that PBLH is not necessarily negatively correlated with pollutant concentration (Miao et al., 2021). In particular, turbulence barrier effect (i.e., it means turbulence may disappear at certain heights forming a laminar flow as if there is a barrier layer hindering the transmission up and down during the heavy pollution episodes) can affect the vertical distribution of pollutants (Ren et al., 2021), which makes the relationship between pollutant and PBLH more uncertain. The PBLH can also be diagnosed by the boundary layer parameterization schemes in the model, but the PBLH does not directly determines the effective diffusion of pollutants (Jia and Zhang, 2020; Jia et al., 2021a). Instead, vertical diffusion and mixing of pollutants are directly determined by turbulent diffusion coefficient (TDC), and the diagnosis of PBLH may affect the calculation of TDC. Previous studies have analyzed a number of pollution cases using process analysis methods (Xing et al., 2017; Gao et al., 2018; Chen et al., 2019). The results showed that, for a pollution event, emissions and turbulent diffusion have the greatest contribution to pollutant concentration. The evolution of pollutants is mainly controlled by turbulent diffusion, when emissions are unchanged for a short period. Meanwhile, the contributions of dry deposition, advection transport and chemistry cannot be ignored. Therefore, more realistic turbulent diffusion characteristics are extremely important for the simulation of pollutant concentration in the model.

To date, a number of issues remain to be addressed in the model, especially turbulent diffusion processes of all scalars (including active and passive scalars) are dealt with in a unified manner in the mesoscale model. Only a few studies have shown that the meteorological fields and pollutants can be changed by adjusting the minimum value of TDC (Savijarvi et al., 2002; Wang et al., 2018; Du et al., 2020; Liu et al., 2021), increasing turbulent kinetic energy (TKE) (Foreman and Emeis, 2012) and modifying experiment expressions (Sušelj and Sood, 2010; Huang and Peng, 2017). Recently, Jia et al. (2021b) obtained the TDC of particles using high-resolution vertical flux data of particles based on the mixing length theory. Additionally, this TDC has been embedded

into the WRF-Chem model to calculate the PBL mixing process of pollutants separately. This work has initially improved the overestimation of pollutant concentration at night in winter 2016 in Eastern China. However, a series of heavy pollution incidents have occurred and attracted much attention since 2013 (Miao et al., 2019). Therefore, we conducted a series of simulations for the heavy pollution periods in winter from 2013 to 2017 in this study. The difference between this study and previous work is that previous work focused on the observational analysis, while this study mainly explores the influence of turbulent diffusion on pollutant concentration in the mesoscale model.

2 Data and methods

2.1 Data

In this study, the aerosol pollution level is denoted by the hourly surface $PM_{2.5}$ concentration that is available from the official website of the China National Environmental Monitoring Center from 1 January 2013 to 31 January 2017. $PM_{2.5}$ concentration stations increased from 35 cities in 2013(illustrated by red dots in Fig. 1b) to 78 cities in 2017(illustrated by black dots in Fig. 1b) in Eastern China. In addition to $PM_{2.5}$ observations, the hourly concentrations of CO were acquired from the National Air Quality real-time publication platform (http://106.37.208.233:20035, last access: 20 May 2021). Meanwhile, the hourly meteorological observation data (a total of 401 stations), including temperature, pressure, relative humidity, wind and visibility from the national automatic weather stations (AWS) provided by the National Meteorological Information Center of China Meteorological Administration (NMICMA) (illustrated by gray crosses in Fig. 1b). The time period of the data selected is from 1 January 2013 to 31 January 2017. In addition, the turbulent diffusion of particles is calculated using high-frequency turbulence data, and observational turbulence data are obtained from the Pingyuan County Meteorological Bureau (37.15°N, 116.47°E), Shandong Province, China from 27 December 2018 to 8 January 2019 (illustrated by orange triangle in Fig. 1b). The experiment station is in the southern suburbs of Dezhou city, and flat farmland

around this station (Fig. S1 and Fig. 2 in Ren et al., 2020), thus, the roughness length is considered to be zero. Identical eddy-covariance systems were operated, including three-dimensional sonic anemometer-thermometer (IRGASON, Campbell Scientific, USA) and CO_2/H_2O open-path gas analyzer (LI7500, LI-COR, USA). These instruments measured three components of wind speed, potential temperature, water vapor and CO_2 concentrations with a frequency of 10 Hz. The turbulence data finally was split into 30-min segments. A continuous particle measuring instrument E-sampler (Met One) and a high-frequency sampling visibility sensor CS120A (Campbell Scientific, USA) were used to obtain $PM_{2.5}$ mass concentration every minute and visibility of 1 Hz. The calculation of 30-min vertical flux of $PM_{2.5}$ is based on the nonlinear relationship between $PM_{2.5}$ concentration and visibility (Ren et al., 2020). The $PM_{2.5}$ concentration, temperature, wind speed at approximately 60 and 10 m were used to compute the vertical gradient of each variable. Considering the interference with the early time of the GPS sounding balloons taking off, the $PM_{2.5}$ concentration near the ground would be uncertain. Thus, we selected 10 m as the lower height to avoid that. Based on the constant flux layer hypothesis, the upper level should be within the surface layer. To facilitate the calculation, we rounded the height difference to 50 m. Finally, 60 m was selected to be higher level to compute the vertical gradient of each variable.

Detailed background and calculation principle of this method were presented in Ren et al. (2020), so we only describe key steps. Firstly, we separate $PM_{2.5}$ concentration (c) and visibility datasets (V) into mean and turbulent deviations (i.e., $c = \bar{c} + c'$ and $V = \bar{V} + V'$). Secondly, we get the fitted coefficients by using exponential correlation (i.e., a and b) between the $PM_{2.5}$ concentration and visibility (i.e., $c = a \cdot V^b$). Thirdly, combining the first two steps, we can get the turbulent fluctuations of $PM_{2.5}$ concentration (i.e., $c' = a \cdot (\bar{V} + V')^b - \bar{c}$). Finally, we use fluctuations of vertical velocity (i.e., w') and of $PM_{2.5}$ concentration (i.e., c') to calculate the vertical flux of

135 PM$_{2.5}$ (i.e., $\overline{w'c'}$). The observed particle flux is used to calculate the Richardson function of particles later.

To illustrate the influence of the PBL height (PBLH) on the PM$_{2.5}$ pollution, soundings collected at the Fuyang site (32.54°N,115.5°E) and the Anqing site (30.37°N,116.58°E) (illustrated by yellow pluses in Fig. 1b) for the period 2013-2017 were analyzed. These

140 two stations are equipped with L-band radiosonde systems (Jia et al., 2021c), which proved a fine resolution (1 Hz) profiles of temperature, relative humidity and wind speed two times (0800 and 2000 BJT) a day during winter. The Richardson number method is used to calculate the PBLH (Miao et al., 2018). The height at which the Richardson number equals 0.25 is defined as the PBLH, which is consistent with the

145 definition of simulation.

2.2 Numerical simulation

Long-term three-dimensional simulation experiments are enforced using the Weather Research and Forecasting model coupled with Chemistry (WRF-Chem version 3.9.1) (Grell et al., 2005) in this study from the winter of 2013 to 2017, when Eastern China

150 frequently experienced severe and persistent aerosol pollution events. One month for each winter from 2013 to 2017 was selected, and a total of four months were confirmed, which are January 2013, December 2014, December 2015 and January 2017, respectively. The anthropogenic emissions of BC, OC, CO, NH$_3$, NO$_x$, PM$_{2.5}$, PM$_{10}$ and volatile organic compounds (VOCs) are set based on the latest monthly Multi-

155 resolution Emission Inventory for China (MEIC) from 2013 to 2017 are provided by Tsinghua University, with a resolution of 0.25°×0.25° (http://meicmodel.org/, last access: 20 May 2021). The model domain was centered over Eastern China with a horizontal resolution of 33 and 6.6 km (Fig. 1a). The model top was set to the 50 hPa level, and 48 vertical layers were configured below the top. To resolve the PBL

160 structure, 21 vertical layers were set below 2 km (i.e., the specific setting of vertical levels is σ= 1.000, 0.997, 0.994, 0.991, 0.988, 0.985, 0.980, 0.975, 0.970, 0.960, 0.950,

0.940, 0.930, 0.920, 0.910, 0.895, 0.880, 0.865, 0.850, 0.825, 0.800). The physics parameterization schemes selected for this study included the Morrison double-moment microphysics scheme (Morrison et al., 2009), RRTMG longwave/shortwave radiation schemes (Iacono et al., 2008), MM5 similarity surface layer scheme (Jiménez et al., 2012), Noah land surface scheme (Chen and Dudhia, 2001), Singer-layer UCM scheme (Kusaka et al., 2001), CLM4.5 lake physics scheme (Subin et al., 2012; Gu et al., 2015), ACM2 planetary boundary layer scheme (Pleim, 2007), Grell-3D cumulus scheme (Grell and Devenyi, 2002). And the chemical mechanism is the RADM2-MADE/SORGM scheme (Ackermann et al., 1998; Schell et al., 2001). The initial and boundary conditions of meteorological fields were set up using the National Centers for Environmental Prediction (NCEP) global final (FNL) reanalysis data, with a resolution of $1°×1°$ (https://rda.ucar.edu/datasets/ds083.2/, last access: 20 May 2021). And the initial and boundary conditions of chemical fields were configured using the global model output of the Model for Ozone and Related Chemical Tracers (MOZART) (http://www/acom.ucar.edu/wrf-chem/mozart.shtml, last access: 20 May 2021).

Figure 2 shows the flow chart of the main program related to the turbulent diffusion coefficient. Simulation using abovementioned configurations is referred to as the original runs. In the original PBL parameterization scheme, TDCs of heat and momentum are different (i.e., $K_h \neq K_m$). The turbulent mixing process of pollutants is considered to be similar to that of heat, which supposes the turbulent diffusions of particles and heat are identical (i.e., $K_h=K_c$) (Fig. 2a). While in the new scheme, the turbulent mixing process of pollutants is calculated by the TDC of particles (i.e., K_c), which is different from TDC of heat (i.e., $K_h \neq K_c$). These improved experiments are regarded as the new runs hereafter (Fig. 2b). All simulations included a total of eight months. The 91-h simulation is conducted beginning from 0000UTC of three days ago for each day (i.e., 248 simulation experiments), the first 64-h of each simulation is considered as the spin-up period, the next 24-h is used for further analysis and the remaining 3-h is discarded (e.g., run one simulation from December 29, 0000 UTC

190   (0800 BJT) to January 01, 1800 UTC (January 02, 0200 BJT), and in total 91 hours.
We need the results from the January 01, 0000 BJT to 2300 BJT. From December 29, 0800 BJT to December 31, 2300 BJT is considered as the spin-up period (in total 64-h), and the results from January 02, 0000 BJT to 0200 BJT is discarded).

2.3 Calculation principle of turbulent diffusion of particles

195   Considering that the pollution is usually accompanied by the stable boundary layer (SBL), and the simulation results of pollutant concentration are poor in the SBL at night. Thus, we mainly modify the program of the stable boundary layer, while for the unstable boundary layer, we still use the default program of the original scheme (Figure 2). Although the turbulent vertical mixing and dry deposition are calculated in the same

200   program in WRF-Chem, we only modified the turbulent diffusion in the new scheme. Here, we briefly describe the information about dry deposition. We adopt the MADE/SORGAM aerosol scheme, in which the dry deposition is calculated based on the Binkowski's method (Binkowski and Shankar, 1995). The dry deposition velocity (V_d) can be expressed as $V_d = V_g + 1/(R_a + R_s + R_a \cdot R_s \cdot V_g)$, where V_g is the

205   gravitational settling velocity, R_a is the aerodynamic resistance and R_s is the canopy resistance.

The TDC is parameterized by the mixing length (l) and the function of Richardson number ($f(Ri)$) based on Mixing length theory, that is

$$K = 0.01 + \sqrt{ss} \cdot l^2 \cdot f(Ri) \qquad (1)$$

where ss is the wind shear (i.e., $ss = (\partial u/\partial z)^2 + (\partial v/\partial z)^2$), 0.01 refers to the minimum

210   value of TDC in the model. The minimum value of TDC remains unchanged in the new scheme. The mixing length formula (i.e., $l = \kappa z/(1 + \kappa z/\lambda)$, $\lambda=80$) proposed by Blackadar (1962), and it is widely used in the model (Louis, 1979; Lin et al., 2008; Pleim, 2016). Ri is the gradient Richardson number (i.e., $Ri = (g/\overline{\theta_v})\partial\overline{\theta_v}/\partial z \left[(\partial\overline{u}/\partial z)^2 + (\partial\overline{v}/\partial z)^2 \right]$, where z is the observation height, g is the

gravity, θ_v is the virtual potential temperature, u and v are the component of wind), which is approximated in finite difference form and the resulting parameter is sometimes referred to as the bulk Richardson number (Garratt, 1992). For example, Louis et al. (1982) shows the Ri is the bulk Richardson number, but the expression is the form of gradient Richardson number (Eq. (5) in Louis et al., 1982). Many previous studies have shown various functions of Richardson number, which represent the different situations of turbulence. Here, we mainly compare the similarities and differences between the turbulent diffusion of momentum, heat and particles in the model.

(i) For the stable conditions (i.e., $Ri \geq 0$), Esau and Byrkjedal (2007) suggested:

$$f_h = (1 + 10Ri + 50Ri^2 + 5000Ri^4)^{-1} + 0.0012 \qquad (2)$$

$$f_m = 0.8f_h + 0.00104 \qquad (3)$$

where f_h and f_m denote the functions of heat and momentum, respectively, and these functions have been existed in the original model. We added an additional function of particles into the model, that is

$$f_c = (1 + 66.6Ri)^{-1} \qquad (4)$$

which is used to denote the turbulent mixing process of particles within the PBL. When Ri is greater than ~0.2, the TDC of particles is greater than that of heat, which may reduce pollutant concentration. With the increase of instability, the TDC of particles is gradually smaller than that of heat, which theoretically leads to the increase of pollutant concentration. For detailed analysis and comparison of functions, please refer to Jia et al. (2021b).

(ii) For the unstable conditions (Ri<0):

$$f_h = f_c = (1 - 25Ri)^{1/2} \qquad (5)$$

$$f_m = \text{Pr} \cdot f_h \qquad (6)$$

where the TDC of particles is still equal to that of heat (i.e., $K_c = K_h$), while the TDC of momentum is calculated by turbulent Prandtl number (i.e., Pr, Pr=0.8).

There are several important information about the TDC of particles that need to be illustrated. (1) Turbulent diffusion of particles calculated by the explicit local gradient to represent the PBL mixing process of particles, which are more suitable in the stable boundary layer (SBL) (Mahrt and Vickers, 2003). (2) The uncertainty of turbulent diffusion coefficient calculated by PBLH and the Monin-Obukhov similarity theory (MOST) at night is large, which have been avoided in the new scheme. Meanwhile, the computational efficiency based on mixing length is higher (Li et al., 2010), and it is easier to apply to the forecasting models in the future. (3) Turbulent diffusion of particles is used to evaluate the PBL mixing process of pollutants separately, which can affect the simulation results of pollutants and not influence the simulation results of meteorological parameters.

3 Evaluation of PM$_{2.5}$ concentration simulation

Based on the TDC relationship of particles in the previous study (Jia et al., 2021b), this study applies this relationship to a long-term scale simulation for verification. Figure 3 show the average value of simulated and observed PM$_{2.5}$ concentration at night (i.e., from 18:00 on the first day to 07:00 on the second day) from 2013 to 2017, and the simulation results can better reproduce the distribution of pollutant concentration (i.e., represented by the red dashed circle). However, the PM$_{2.5}$ concentration was overestimated to varying degrees in Eastern China (i.e., indicated by the green dashed circle), and the mean relative bias (RB) of the region is as high as 11.8% (2013), 48% (2014), 23.8% (2015) and 20.9% (2017), respectively (Fig. 3i-l). In addition, we also found that the pollutant concentrations are underestimated in Beijing (BJ) and along the Taihang Mountains (Mt. Taihang) (i.e., indicated by the purple irregular circle), but overestimated in Tianjin (TJ) (Fig. 3i-l). What are the reasons why the pollutant concentration simulated by the same model is different in each region? What are the different effects of turbulent diffusion in different regions? These issues will be further explained later, and this section primarily evaluates the simulation results of the pollutant concentration. Compared to the original scheme, the new scheme improves

265   the situation where the pollutant concentration is overestimated at night in Eastern China (Fig. 4a-d). The degree of overestimation of the pollutant concentration is reduced, and the mean relative bias of the new scheme is 3.5% (2013), 31% (2014), 12.8% (2015) and 9.2% (2017), respectively (Fig. 4e-h). As well, the mean absolute bias is decreased by 8.3% (2013), 17% (2014), 11% (2015) and 11.7% (2017),

270   respectively (Fig. 4i-l). In summary, compared with the original scheme, the new scheme can generally improve the overestimation of pollutant concentration in Eastern China, which is due to the changes in turbulent diffusion. For the above stations where the pollutant concentration was underestimated in the original scheme, the pollutant concentration will be further underestimated with the increase in turbulent diffusion.

275   However, this underestimation cannot be avoided because there is an opposite phenomenon in the pollutant concentration in the two regions. We can only look at the differences in the two regions from other perspectives (see section 4 for details), as the model is fraught with uncertainties.

To better evaluate the model performance, figure 5 shows the Taylor diagram of hourly

280   $PM_{2.5}$ concentration, and the black (red) dots indicate original (new) simulation results at all stations from 2013 to 2017. The statistical results have a consistent feature, that is, the worse the simulation results of the original scheme are, the more obvious improvement of the new scheme becomes (arrows indicate improved stations in the Fig. 5). The results indicate that the pollutant concentrations are not improved to the same

285   degree at all stations. When the simulation of pollutant concentration is overestimated in the original scheme, the new scheme can significantly reduce the degree of overestimation. While the simulation of pollutant concentration is underestimated in the original scheme, the new scheme cannot further underestimate and the degree of re-underestimate is not obvious (Fig. 5 and Fig. S2). And the mean value of standard

290   deviation (normalized) are decreased by 0.2 (2013), 0.28 (2014), 0.14 (2015) and 0.16 (2017) (Fig. 5). As a whole, the new scheme can significantly improve the common phenomenon of overestimated pollutant concentration at night in Eastern China (Fig. 5).

As turbulent diffusion increases, the pollutant concentration gradually decreases. Where do the reduced pollutants go? Did it spread to the surrounding area in the horizontal direction or diffuse to the upper level in the vertical direction? This question warrants a more in-depth discussion. It can be seen from Figure 4 that the reduction in pollutant concentration is a regional synchronous change and there is no regular concentration gradient in the horizontal direction. Therefore, we should also pay more attention to the changes in the vertical direction. Theoretically, increasing turbulent diffusion can reduce the pollutant concentrations near the surface-layer, and the pollutants can be more fully mixing in the vertical direction, leading to lower pollutant concentration in the near surface-layer and higher in the upper layer. As we expected, the pollutant concentration is reduced in the surface-layer and increased in the upper layer at night in Eastern China (Fig. 6, Fig. S3-S5), which is consistent with the theory.

4 Uncertainty analysis

4.1 Meteorological parameters

Depending on high-frequency particle flux, the TDC of particles has been added into the model to compute the turbulent mixing process of particles separately. Compared with previous studies about the improvement of parameterization scheme, the greatest strengths of the new scheme is that not only improves the simulation results of pollutant concentration, but also does not deteriorate the simulation results of other parameters. To verify the new scheme does not affect the simulation results of the meteorological parameters, the simulation results of the near-surface meteorological elements (i.e., 2-m temperature, 2-m relative humidity and 10-m wind speed) between original and new schemes have been compared and analyzed. It can be seen from Figure S6-S8 that the correlation coefficients of meteorological parameters by two schemes are greater than 0.99. Noting that the new scheme does not alter the performance of meteorological fields, which is an advantage of the new scheme. As mentioned earlier, modifying the

320 turbulent diffusion coefficient of heat not only affects the simulation of temperature (Savijarvi and Kauhanen, 2002), but also the results of pollutants (Liu et al., 2021).

Improving the parameterization scheme is a long and tough process, making it difficult to improve the simulation results of all parameters at the same time. When the simulation results of one parameter are improved, we should first ensure that the

325 simulation results of other parameters are not deteriorated. Then, we will work on improving other parameters. Although the aerosol-radiation two-way feedback process was considered in the WRF-Chem model, the change in $PM_{2.5}$ concentration caused by radiation feedback is only a few percentage (Li et al., 2017; Wu et al., 2019; Gao et al., 2020). We should focus more on the impact of turbulence on aerosol pollution, and

330 some turbulent characteristics (e.g., turbulence barrier effect and turbulent intermittency) can be taken into consideration during heavy pollution episodes (HPEs), and reflecting a more realistic evolution process of pollutant concentration. We will further clarify the relationship between particles, momentum and heat transport through observational data, so as to lay the foundation for model improvement.

335 ## 4.2 PBL height

Although PBL height (PBLH) is widely used to determine the effective air volume and atmospheric environmental capacity for pollutant diffusion, various methods diagnose different PBLH, which reinforces uncertainty about the PBLH as a criterion. When there is a transport stage with a high wind speed during HPEs, the mechanical

340 turbulence is strong, the pollutant concentration and PBLH increase simultaneously (Jia et al., 2021c; Miao et al. 2021). Therefore, the relationship between PBLH and $PM_{2.5}$ pollution is intricate. The impact of PBLH is ultimately represented through the TDC in the model, as PBLH is used to calculate the TDC (Jia et al., 2021b). And artificial changing PBLH can also affect the simulation of pollutant concentration. If the

345 simulation error in pollutant concentration is caused by PBLH, that is the pollutant concentration is overestimated and PBLH should be underestimated. However, PBLH

is reproduced well by the model, and the model does not underestimate PBLH (Fig. 7). Anqing is located in the mountain corridor, the simulation results of PBLH (Index of agreement, IOA=0.49~0.81) are slightly worse than that in Fuyang (IOA=0.63~0.85).

350   Therefore, various factors can influence the calculation of PBLH.

A more accurate PBLH can reduce some uncertainty in the model, but how to apply the accurate PBLH through observation to the model is a thorny problem. For example, the turbulence barrier effect modifies the mixing height of pollutants (Ren et al., 2021), which cannot be reflected in the model and can lead to deviation in the simulation of

355   pollutant concentration. The new scheme does not disturb the simulation results of meteorological fields, thus, does not affect the simulation results of PBLH (Fig. S9). The simulation results of pollutant concentrations are improved under the similar PBLH, which further demonstrates that the simulation of pollutant concentration is not only controlled by PBLH, but also influenced by turbulent diffusion. Finally, turbulent

360   diffusion controls the mixing of pollutant concentration and the evolution of meteorological parameters.

4.3 Influence of other processes

Overestimation of pollutant concentrations has been improved in Eastern China, but there are also some stations in northern China where pollutant concentrations are

365   underestimated (Fig. 3i-l). Therefore, the stratification is more stable in the most part of nighttime in Eastern China (Ri is greater than ~0.2, based on the fitting function in Jia et al., 2021b), while the stratification tends to the weakly stable/unstable at the same time in the mountainous area with complex terrain. These stations (i.e., Hebei and Beijing) are mostly located in the east of the Taihang Mountains and the south of the

370   Yan Mountains (Fig. 8). For example, in December 2016, the pollutant concentrations of all stations in Beijing were not underestimated. Jia et al. (2021b) found that the pollutant concentrations of two stations located in the south of Beijing (i.e., blue dots in Fig. S2 in Jia et al., 2021b) are well reproduced by the model. This phenomenon also

occurred in 2013-2017 (Fig. 8) with pollutant concentrations significantly underestimated at some stations near the mountainous area. The boundaries of overestimated and underestimated sites are pronounced in Beijing-Tianjin-Hebei region (white dashed in Fig. 8), and the pollutant concentration is overestimated at some stations, which are away from the mountainous area (i.e., Tianjin and southeast of Hebei). Meanwhile, the TDC of particles in the new scheme is greater than that of heat in the original scheme in Eastern China (i.e., red dashed circle in Fig. 9i-l), that is, the increased turbulent diffusion improves the overestimation of pollutant concentration in this area. Compared to the original scheme, the increase in TDC in the new scheme is attributed to the change in $f(Ri)$ when other physical quantities remain unchanged. Furthermore, we found that the TDC in the new scheme is much smaller than that in the original scheme in the mountainous area (i.e., green irregular circle in Fig. 9). Theoretically, the reduced TDC is expected to increase the pollutant concentration, and improve the underestimation of pollutant concentration in the original scheme. Disappointingly, the change in TDC does not improve the underestimation of pollutant concentration in the mountainous area (Fig. 8, 9i-l), indicating that the change in turbulent diffusion is not sensitive to the pollutant concentration in the mountainous area.

In addition to the main influencing factors of emission and turbulent diffusion, advection transport, chemistry processes and dry deposition can also affect the simulation of pollutant concentration. Given that we are using the latest emissions source inventory, it is impossible to use other more elaborate inventories to quantify the uncertainty caused by emissions. Advection process, is strongly related to wind and $PM_{2.5}$ concentration gradients from upwind areas to downwind areas (Gao et al., 2018). Figure 10 shows that the simulation results of wind speed, and we found that the wind speed is overestimated in the whole simulation area, which is also the systematic deviation of the model (Jia and Zhang, 2020). However, there are regional differences in the overestimation of wind speed, which is more obvious in areas with complex terrain (framed by purple lines in Fig. 10). Jimenez and Dudhia (2012) indicated that

the overestimation of wind speed may be caused by the incorrect describe sub-grid surface roughness. For the purple rectangle region, although the wind speed is overestimated, there is no evident wind speed gradient and pollutant concentration gradient (Fig. 3a-d, 10a-d). Thus, the effect of advection is insignificant. While for the irregular purple region, we can see that the obvious wind speed gradient and pollutant concentration gradient (Fig. 3a-d, 10a-d). In the northwest of the irregular purple area, clean air will pass through this area under the control of stronger northwesterly wind. Consequently, this area is extremely susceptible to advection transport, so that the pollutant concentration has been underestimated in this area. We should pay more attention to the improvement of wind field simulation in complex terrain. We expect that the simulation of wind field to be improved, which will lead to an improvement in pollutant concentration in this area.

Chemistry process, i.e., the $PM_{2.5}$ concentration contribution caused by secondary transformation, was negligible in this study, and is not mentioned further in this paper. Whether the simulation of chemical components has been improved, it cannot be properly verified because of the lack of observational data. Although the simulation results of $PM_{2.5}$ components cannot be evaluated, CO, as a representative of primary pollutants, can be compared with the observations. Results from new scheme with TDC of particles are more consistent with the observations than the original scheme (Fig. S10), which supports the improvement of $PM_{2.5}$ concentration (Fig. 5 and S10). Moreover, the dry deposition process of particles is also extremely important (Zhang et al., 2001; Farmer et al., 2021). The turbulent mixing and dry deposition processes belong to the same main program in the mesoscale model. However, as particle size increases, particle inertia and gravity cannot be neglected, but these inertia and gravity effects are neglected for particles smaller than 10 µm in diameter (Fratini et al., 2007). As a result, we did not involve the influence of gravity on pollutant concentration in this study. Petroff and Zhang (2010) showed that according to the method in Zhang et al. (2001), the dry deposition can be overestimated, especially for fine particles. Special attention must be paid to the fact that the overestimation of dry deposition affects the

distribution of pollutant concentration. Therefore, the choice of dry deposition scheme also needs to be carefully considered, because this process is also very important for the evolution of pollutants. In the future, long-term simulation results should be used to verify the difference in aerosol process decomposition in detail.

5 Conclusions and prospects

At present, the mesoscale model is facing numerous challenges, especially the accurate simulation of pollutant concentration during heavy pollution episodes. One of these challenges is to correctly describe the turbulent mixing process of pollutants. Although the model can reproduce the evolution of pollutants, the simulation of diurnal variation of pollutants is fundamentally flawed, especially at night. Errors in the estimation of pollutant concentration are primarily caused by defects in the turbulent mixing of pollutants in the model. Actually, a difference exists between the turbulent transport of heat and particles, which inspires us to deal with the turbulent diffusion of heat and particles separately. Therefore, based on the turbulent diffusion expression of particles proposed by Jia et al., 2021b, we demonstrated the improvement of pollutant concentration in winter from 2013 to 2017, and the uncertainty factors are also analyzed in the model.

The original scheme overestimates the surface $PM_{2.5}$ concentration by 11.8% (2013), 48% (2014), 23.8% (2015) and 20.9% (2017) at night, respectively. The new scheme has improved the overestimation of the surface $PM_{2.5}$ concentration in eastern China at night, and the mean absolute bias of the region can be reduced by 8.3% (2013), 17% (2014), 11% (2015) and 11.7% (2017), respectively. In the horizontal direction, the pollutant concentration showed regional synchronous changes. Consequently, the pollutant concentration is reduced near the surface layer and better mixed in the entire layer, and increasing the pollutant concentration in the upper level. Moreover, the new scheme not only improves the simulation of pollutant concentration, but also does not deteriorate the simulation of other meteorological parameters. Although PBLH affects

the diffusion of pollutants, the simulation of pollutant concentration is not specifically controlled by PBLH. It should be noted that TDC has a negligible impact on the simulation of pollutant concentration at some stations with complex topography. Meanwhile, advection transport may dominate the evolution of pollutant concentration in mountainous area. The simulation results of $PM_{2.5}$ components cannot be evaluated, due to lack of observational data. CO, however, as a representative of primary pollutants, can be compared with observations. Results from new scheme are more consistent with the observations than the original scheme, which supports the improvement of the $PM_{2.5}$ concentration.

The coefficient of function in this study should be discussed given the sample size of data, but we hope the new scheme can provide promising guidance during heavy pollution episodes. The turbulent transport mechanism and turbulence parameterization constitute a complex topic (Lemon et al., 2019; Couvreux et al., 2020; Edwards et al., 2020), and beyond this, other processes (or other parameters) require in-depth understanding and exploration (Zhang et al., 2001; Seinfeld et al., 2016; Shao et al., 2019; Emerson et al., 2020). Therefore, more research may shed more light on the turbulent mixing process and transport mechanisms of pollutants during the heavy pollution episodes, especially on the experimental side (e.g., carry out extensive measurement campaigns).

Data availability

The surface $PM_{2.5}$ concentration, meteorological data, turbulent datasets and turbulent flux data of $PM_{2.5}$ are available by request (xiaoye@cma.gov.cn).

Author contributions

Development of the ideas and concepts behind this work was performed by all the authors. Model execution, data analysis and paper preparation were performed by WJ and XZ with feedback and advice.

Competing interests

The authors declare that they have no conflict of interest.

Acknowledgments

The authors would like to acknowledge the Tsinghua University for the support of emission data.

490 **Financial support**

This research is supported by NSFC Major Project (42090030), NSFC Project (U19A2044).

References

Ackermann, I. J., Hass, H., Memmesheimer, M., Ebel, A., Binkowski, F. S., and Shankar, U.: Modal

495   aerosol dynamics model for Europe, Atmos. Environ., 32, 2981–2999, https://doi.org/10.1016/S1352-2310(98)00006-5, 1998.

An, Z., Huang, R., Zhang, R., Tie, X., Li, G., Cao, J., Zhou, W., Shi, Z., Han, Y., Gu, Z., and Ji, Y.: Severe haze in northern China: A synergy of anthropogenic emissions and atmospheric processes, P. Natl. Acad. Sci. USA, 116, 8657–8666, https://doi.org/10.1073/pnas.1900125116, 2019.

500 Blackadar, A. K.: The vertical distribution of wind and turbulent exchange in a neutral atmosphere, J. Geophys. Res., 67, 3095–3102, https://doi.org/10.1029/JZ067i008p03095, 1962.

Chen, F., and Dudhia, J.: Coupling an advanced land surface – hydrology model with the Penn State – NCAR MM5 modeling system. Part I: model implementation and sensitivity, Mon. Wea. Rev., 129, 569–585, https://doi.org/10.1175/1520-0493(2001)129 < 0587:CAALSH > 2.0.CO, 2, 2001.

505 Chen, L., Zhu, J., Liao, H., Gao, Y., Qiu, Y., Zhang, M., Liu, Z., Li, N., and Wang, Y.: Assessing the formation and evolution mechanisms of severe haze pollution in the Beijing–Tianjin–Hebei region using process analysis, Atmos. Chem. Phys., 19, 10845-10864, https://doi.org/10.5194/acp-19-10845-2019, 2019.

Couvreux, F., Bazile, E., Rodier, Q., Maronga, B., Matheou, G., and Chinita, M. J., Edwards, J., Stratum,

510   B. J. H., van Heerwaarden, C. C., Huang, J., Moene, A. F., Cheng, A., Fuka, V., Basu, S., Bou-Zeid, E., Canut, G., and Vignon, E.: Intercomparison of large-eddy simulations of the Antarctic boundary layer for very stable stratification, Bound.-Lay. Meteorol., 176, 369–400, https://doi.org/10.1007/s10546-020-00539-4, 2020.

Du, Q., Zhao, C., Zhang, M., Dong, X., Cheng, Y., Liu, Z., Hu, Z., Zhang, Q., Li, Y., Yuan, R., and Miao,

515   S.: Modeling diurnal variation of surface $PM_{2.5}$ concentrations over East China with WRF-Chem:

impacts from boundary-layer mixing and anthropogenic emission, Atmos. Chem. Phys., 20, 2839–2863, https://doi.org/10.5194/acp-20-2839-2020, 2020.

Edwards, J. M., Beijaars, A. C., Holtslag, A. A., and Lock, A. P.: Representation of boundary-layer processes in numerical weather prediction and climate models, Bound.-Lay. Meteorol., 177, 511–539, https://doi.org/10.1007/s10546-020-00530-z, 2020.

Emerson, E. W., Hodshire, A. L., Debolt, H. M., Bilsback, K. R., Pierce, J. R., McMeeking, G. R., and Farmer, D. K.: Revisiting particle dry deposition and its role in radiative effect estimates, P. Natl. Acad. Sci. USA, 117, 26076–26082, https://doi.org/10.1073/pnas.2014761117, 2020.

Esau, I. N., and Byrkjedal, Ø.: Application of large eddy simulation database to optimization of first order closure for neutral and stably stratified boundary layers, Bound.-Lay. Meteorol., 125, 207–225, https://doi.org/10.1007/s10546-007-9213-6, 2007.

Farmer, D.K., Boedicker, E.K. and DeBolt, H.M.: Dry Deposition of Atmospheric Aerosols: Approaches, Observations, and Mechanisms, Annu. Rev. Phys. Chem. 72, 16.1–16.23, https://doi.org/10.1146/annurev-physchem-090519-034936, 2021.

Foreman, R. J., and Emeis, S.: A Method for Increasing the Turbulent Kinetic Energy in the Mellor–Yamada–Janjić Boundary-Layer Parametrization, Bound.-Lay. Meteorol., 145, 329–349, https://doi.org/10.1007/s10546-012-9727-4, 2012.

Fratini, G., Ciccioli, P., Febo, A., Forgione, A., and Valentini, R.: Size-segregated fluxes of mineral dust from a desert area of northern China by eddy covariance. Atmos. Chem. Phys., 7, 2839–2854, https://doi.org/10.5194/acp-7-2839-2007, 2007.

Gao, J., Zhu, B., Xiao, H., Kang, H., Pan, C., and Wang, D., and Wang, H.: Effects of black carbon and boundary layer interaction on surface ozone in Nanjing, China, Atmos. Chem. Phys., 18, 7081–7094, https://doi.org/10.5194/acp-18-7081-2018, 2018.

Gao, M., Han, Z., Tao, Z., Li, J., Kang, J.-E., Huang, K., Dong, X., Zhuang, B., Li, S., Ge, B., Wu, Q., Lee, H.-J., Kim, C.-H., Fu, J. S., Wang, T., Chin, M., Li, M., Woo, J.-H., Zhang, Q., Cheng, Y., Wang, Z., and Carmichael, G. R.: Air quality and climate change, Topic 3 of the Model Inter-Comparison Study for Asia Phase III (MICS-Asia III) – Part 2: aerosol radiative effects and aerosol feedbacks, Atmos. Chem. Phys., 20, 1147–1161, https://doi.org/10.5194/acp-20-1147-2020, 2020.

Garratt, J.: The atmospheric boundary layer, Cambridge, UK, 37, 1992.

545   Grell, G. A., and Devenyi, D.: A generalized approach to parameterizing convection combining ensemble and data assimilation techniques, Geophys. Res. Lett., 29, 1693, https://doi.org/10.1029/2002GL015311, 2002.

Grell, G.A., Peckham, S.E., Schmitz, R., McKeen, S.A., Frost, G., Skamarock, W.C., and Eder, B.: Fully coupled "online" chemistry within the WRF model. Atmos. Environ., 39, 6957–6975.
550   https://doi.org/10.1016/j.atmosenv.2005.04.027, 2005.

Gu, H., Jin, J., Wu, Y., Ek, M. B., and Subin, Z. M.: Calibration and validation of lake surface temperature simulations with the coupled WRF-lake model, Clim. Change., 129, 471–483, https://doi.org/10.1007/s10584-013-0978-y, 2015.

Huang, Y., and Peng, X.: Improvement of the Mellor–Yamada–Nakanishi–Niino Planetary Boundary-
555   Layer Scheme Based on Observational Data in China, Bound.-Lay. Meteorol., 162, 171–188, https://doi.org/10.1007/s10546-016-0187-0, 2017.

Iacono, M. J., Delamere, J. S., Mlawer, E. J., Shephard, M. W., Clough, S. A., and Collins, W. D.: Radiative forcing by long-lived greenhouse gases: calculations with the AER radiative transfer models, J. Geophys. Res.: Atmos., 113, D13103. https://doi.org/10.1029/2008JD009944, 2008.

560   Jia, W., and Zhang, X.: The role of the planetary boundary layer parameterization schemes on the meteorological and aerosol pollution simulations: A review, Atmos. Res., 239, 104890, https://doi.org/10.1016/j.atmosres.2020.104890, 2020.

Jia, W., Zhang, X., and Wang, Q.: Assessing the pollutant evolution mechanisms of heavy pollution episodes in the Yangtze-Huaihe valley: A multiscale perspective, Atmos. Environ., 244, 117986,
565   https://doi.org/10.1016/j.atmosenv.2020.117986, 2021a.

Jia, W., Zhang, X., Zhang, H., and Ren, Y.: Application of turbulent diffusion term of aerosols in mesoscale model, Geophys. Res. Lett., 48, e2021GL093199, https://doi.org/10.1029/2021GL093199, 2021b.

Jia, W., Zhang, X., Wang, J., Yang, Y., and Zhong, J.: The influence of stagnant and transport types
570   weather on heavy pollution in the Yangtze-Huaihe valley, China, Sci. Total Environ., 792, 148393, https://doi.org/10.1016/j.scitotenv.2021.148393, 2021c.

Jiménez, P.A., Dudhia, J.: Improving the representation of resolved and unresolved topographic effects on surface wind in the WRF model, J. Appl. Meteorol. Climatol., 51, 300–316, https://doi.org/10.1175/JAMC-D-11-084.1, 2012.

575 Jiménez, P. A., Dudhia, J., González–Rouco, J. F., Navarro, J., Montávez, J. P., and García–Bustamante E.: A revised scheme for the WRF surface layer formulation, Mon. Wea. Rev., 140, 898–918, https://doi.org/10.1175/MWR-D-11-00056.1, 2012.

Kusaka, H., Kondo, H., Kikegawa, Y., and Kimura, F.: A simple single-layer urban canopy model for atmospheric models: comparison with multi-layer and slab models. Bound.-Lay. Meteorol., 101,
580 329–358, https://doi.org/10.1023/a:1019207923078, 2001.

LeMone, M. A., Angevine, W. M., Bretherton, C. S., Chen, F., Dudhia, J., Fedorovich, E., Katsaros, K. B., Lenschow, D. H., Mahrt, L., Patton, E. G, Sun, J. L., Tjernström, M., and Weil, J.: 100 Years of progress in boundary layer meteorology, Meteorol. Mono., 59, 9.1–9.85, https://academic.microsoft.com/paper/2935666247, 2019.

585 Li, M., Wang, T., Xie, M., Zhuang, B., Li, S., Han, Y., and Chen, P.: Impacts of aerosol-radiation feedback on local air quality during a severe haze episode in Nanjing megacity, eastern China, Tellus B: Chem. Phys. Meteorol., 69, 1339548, https://doi.org/10.1080/16000889.2017.1339548, 2017.

Li, Y., Gao, Z., Lenschow, D. H., and Chen, F.: An improved approach for parameterizing surface-layer turbulent transfer coefficients in numerical models, Bound.-Lay. Meteorol., 137, 153–165,
590 https://doi.org/10.1007/s10546-010-9523-y, 2010.

Lin, J., Youn, D., Liang, X., and Wuebbles, D. J.: Global model simulation of summertime U.S. ozone diurnal cycle and its sensitivity to PBL mixing, spatial resolution, and emissions, Atmos. Environ., 42, 8470–8483, https://doi.org/10.1016/j.atmosenv.2008.08.012, 2008.

Liu, C., Huang, J. Hu, X.-M., Hu, C., Wang, Y., Fang, X., Luo, L., Xiao, H., and Xiao, H.: Evaluation of
595 WRF-Chem simulations on vertical profiles of $PM_{2.5}$ with UAV observations during a haze pollution event, Atmos. Environ., 252, 118332, https://doi.org/10.1016/j.atmosenv.2021.118332, 2021.

Louis, J.: A parametric model of vertical eddy fluxes in the atmosphere, Bound.-Lay. Meteorol., 17, 187–202, https://doi.org/10.1007/BF00117978, 1979.

Louis, J., Tiedtke, M., and Geleyn, J.: A short history of the PBL parameterization at ECMWF, ECMWF,
600 59–79, https://www.ecmwf.int/node/10845, 1982.

Mahrt, L., and Vickers, D.: Formulation of turbulent fluxes in the stable boundary layer, J. Atmos. Sci., 60, 2538–2548, https://doi.org/10.1175/1520-0469(2003)060<2538:FOTFIT>2.0.CO;2, 2003.

Miao, Y., Che, H., Zhang, X., and Liu, S.: Relationship between summertime concurring $PM_{2.5}$ and O_3 pollution and boundary layer height differs between Beijing and Shanghai, China, Environ. Pollut., 605 268, 115775, https://doi.org/10.1016/j.envpol.2020.115775, 2021.

Miao, Y., Li, J., Miao, S., Che, H., Wang, Y., Zhang, X., Zhu, R., and Liu, S.: Interaction between planetary boundary layer and PM2.5 pollution in megacities in China: a review, Curr. Pollut. Rep., 5, 261–271, https://doi.org/10.1007/s40726-019-00124-5, 2019.

Miao, Y., Liu, S., Guo, J., Huang, S., Yan, Y., and Lou, M.: Unraveling the relationships between 610 boundary layer height and PM2.5 pollution in China based on four-year radiosonde measurements, Environ. Pollut., 243, 1186–1195, https://doi.org/10.1016/j.envpol.2018.09.070, 2018.

Morrison, H., Thompson, G., and Tatarskii, V.: Impact of Cloud Microphysics on the Development of Trailing Stratiform Precipitation in a Simulated Squall Line: Comparison of One– and Two– Moment Schemes, Mon. Wea. Rev., 137, 991–1007, https://doi.org/10.1175/2008MWR2556.1, 615 2009.

Petroff, A. and Zhang, L.: Development and validation of a size-resolved particle dry deposition scheme for application in aerosol transport models, Geosci. Model Dev., 3, 753–769, https://doi.org/10.5194/gmd-3-753-2010, 2010.

Pleim, J. E.: A combined local and nonlocal closure model for the atmospheric boundary layer. Part I: 620 model description and testing, J. Appl. Meteorol. Climatol., 46, 1383–1395, https://doi.org/10.1175/JAM2539.1, 2017.

Pleim, J. E., Gilliam, R., Appel, W., and Ran, L.: Recent advances in modeling of the atmospheric boundary layer and land surface in the coupled WRF-CMAQ model, Air Pollution Modeling and its Application XXIV, 391–396, https://doi.org/10.1007/978-3-319-24478-5_64, 2016.

625 Ren, Y., Zhang, H., Wei, W., Cai, X., and Song, Y.: Determining the fluctuation of $PM_{2.5}$ mass concentration and its applicability to Monin–Obukhov similarity, Sci. Total Environ., 710, 136398, https://doi.org/10.1016/j.scitotenv.2019.136398, 2020.

Ren, Y., Zhang, H., Zhang, X., Wei, W., Li, Q., Wu, B., Cai, X., Song, Y., Kang, L., and Zhu, T.: Turbulence barrier effect during heavy haze pollution events, Sci. Total Environ., 753, 142286, 630 https://doi.org/10.1016/j.scitotenv.2020.142286, 2021.

Ren, Y., Zheng, S., Wei, W., Wu, B., Zhang, H., Cai, X., and Song, Y.: Characteristics of the turbulent transfer during the heavy haze in winter 2016/17 in Beijing, J. Meteor. Res., 32, 69–80, https://doi.org/10.1007/s13351-018-7072-3, 2018.

Savijärvi, H., and Kauhanen, J.: High resolution numerical simulations of temporal and vertical variability in the stable wintertime boreal boundary layer: a case study, Theor. Appl. Climaol., 70, 97–103, https://doi.org/10.1007/s007040170008, 2002.

Schell, B., Ackermann, I. J., and Hass, H.: Modeling the formation of secondary organic aerosol within a comprehensive air quality model system, J. Geophys. Res., 106, 28275–28293, https://doi.org/10.1029/2001JD000384, 2001.

Seinfeld, J. H., Bretherton, C., Carslaw, K. S., Coe, H., DeMott, P. J., Dunlea, E. J., Feingold, G., Ghan, S., Guenther, A. B., Kahn, R., Kraucunas, I., Kreidenweis, S. M., Molina, M. J., Nenes, A., Penner, J. E., Prather, K. A., Ramanathan, V., Ramaswamy, V., Rasch, P. J., Ravishankara, A. R., Rosenfeld, D., Stephens, G., and Wood, R.: Improving our fundamental understanding of the role of aerosol-cloud interactions in the climate system, P. Natl. Acad. Sci. USA, 113, 5781–5790. https://doi.org/10.1073/pnas.1514043113, 2016.

Shao, J., Chen, Q, Wang, Y., Lu, X., He, P., Sun, Y., Shah, V., Martin, R. V., Philip, S., Song, S., Zhao, Y., Xie, Z., Zhang, L., and Alexander, B.: Heterogeneous sulfate aerosol formation mechanisms during wintertime Chinese haze events: air quality model assessment using observations of sulfate oxygen isotopes in Beijing, Atmos. Chem. Phys., 19, 6107–6123. https://doi.org/10.5194/acp-19-6107-2019, 2019.

Smedman, A.-S., Högström, U., Hunt, J. C. R., and Sahlée, E.: Heat/mass transfer in the slightly unstable atmospheric surface layer, Q. J. R. Meteorol. Soc. 133, 37–51. https://doi.org/10.1002/qj.7, 2007.

Stull, R. B.: An introduction to boundary layer meteorology, Atmospheric Sciences Library, 6, 206–210, 1988.

Subin, Z. M., Riley, W. J., and Mironov, D.: An improved lake model for climate simulations: Model structure, evaluation, and sensitivity analyses in CESM1, J. Adv. Model. Earth Syst., 4, M02001, https://doi.org/10.1029/2011MS000072, 2012.

Sušelj, K., and Sood, A.: Improving the Mellor–Yamada–Janjić Parameterization for wind conditions in the marine planetary boundary layer, Bound.-Lay. Meteorol., 136, 301–324. https://doi.org/10.1007/s10546-010-9502-3, 2010.

Wang, H., Peng, Y., Zhang, X., Liu, H., Zhang, M., Che, H., Cheng, Y., and Zheng, Y.: Contributions to the explosive growth of $PM_{2.5}$ mass due to aerosol-radiation feedback and decrease in turbulent diffusion during a red alert heavy haze in Beijing-Tianjin-Hebei, China, Atmos. Chem. Phys. 18, 17717–17733. https://doi.org/10.5194/acp-18-17717-2018, 2018.

665 Wu, J., Bei, N., Hu, B., Liu, S., Zhou, M., Wang, Q., Li, X., Liu, L., Feng, T., Liu, Z., Wang, Y., Cao, J., Tie, X., Wang J., Molina, L. T., and Li, G.: Aerosol–radiation feedback deteriorates the wintertime haze in the North China Plain, Atmos. Chem. Phys., 19, 8703–8719, https://doi.org/10.5194/acp-19-8703-2019, 2019.

Xing, J., Wang, J., Mathur, R., Wang, S., Sarwar, G., Pleim, J., Hogrefe, C., Zhang, Y., Jiang, J., Wong,

670 D., and Hao, J.: Impacts of aerosol direct effects on tropospheric ozone through changes in atmospheric dynamics and photolysis rates. Atmos. Chem. Phys., 17, 9869 – 9883, https://doi.org/10.5194/acp-17-9869-2017, 2017.Zhang, H., Zhang, X., Li, Q., Cai, X., Fan, S., Song, Y., Hu, F., Che, H., Quan, J., Kang, L., and Zhu, T.: Research progress on estimation of the atmospheric boundary layer height, J. Meteor. Res., 34, 482–498, https://doi.org/10.1007/s13351-

675 020-9910-3, 2020.

Zhang,.L, Gong, S., Padro, J., and Barrie, L.: A size-segregated particle dry deposition scheme for an atmospheric aerosol module, Atmos. Environ., 35, 549–560, https://doi.org/10.1016/S1352-2310(00)00326-5, 2001.

Zhang, X., Xu, X., Ding, Y., Liu, Y., Zhang, H., Wang, Y., and Zhong, J.: The impact of meteorological

680 changes from 2013 to 2017 on $PM_{2.5}$ mass reduction in key regions in China, Sci. China Earth Sci., 62, 1–18. https://doi.org/10.1007/s11430-019-9343-3, 2019.

Figure 1. (a) Map of terrain height in the two nested model domains. (b) The locations of surface meteorological stations, air quality monitoring stations and sounding stations are marked by the gray crosses, red(black) dots and yellow pluses, respectively. The turbulence data site is denoted by the orange triangle. The red dashed circle indicates the areas of our primary concern.

(a) Original Scheme	(b) New Scheme
WRF-Chem Main Program	**WRF-Chem Main Program**
Call vertical mixing in WRF-Chem	**Call** vertical mixing in WRF-Chem
WRF Main Program	**WRF Main Program**
Get ACM2 scheme variables from WRF	**Get** ACM2 scheme variables from WRF
	Add relevant variables of particles in ACM2 scheme
for i: i_start to i_end	*for* i: i_start to i_end
for k: k_start to k_end	*for* k: k_start to k_end
compute Richardson number (Ri)	compute Richardson number (Ri)
compute wind shear	compute wind shear
compute mixing length scale	compute mixing length scale
define Prandtl number (Pr = 0.8)	define Prandtl number (Pr = 0.8)
define the minimum turbulent diffusion coefficient (K_{min}=0.01)	define the minimum turbulent diffusion coefficient (K_{min}=0.01)
if $Ri \geq 0$	*if* $Ri > 0$
compute stability function of heat ($f_h(Ri)$)	compute stability function of heat ($f_h(Ri)$)
compute stability function of momentum $f_m(Ri)$ by Pr and $f_h(Ri)$	compute stability function of momentum $f_m(Ri)$ by Pr and $f_h(Ri)$
	compute stability function of praticles $f_c(Ri)$
compute turbulent diffusion coefficient of heat (K_h) and momentum (K_m)	compute turbulent diffusion coefficient of heat (K_h), momentum (K_m) and particles (K_c)
else $Ri < 0$	*else* $Ri < 0$
compute K_h	compute K_h
compute K_m by Pr	compute K_m by Pr
	$K_c = K_h$
end	*end*
end	*end*
end	*end*
Get K_h from WRF	**Get** K_c from WRF
Input K_h into vertical mixing in WRF-Chem (Dry deposition remains unchanged)	**Input** K_c into vertical mixing in WRF-Chem (Dry deposition remains unchanged)
Continue vertical mixing	**Continue** vertical mixing

Figure 2. Flow chart of main program for turbulent diffusion coefficient in the (a) original scheme and (b) new scheme.

Figure 3. The average value of (a-d) simulated and (e-h) observed PM2.5 concentration (μg m⁻³) at night, (i-l) the relative bias (RB, %) between simulation and observation, and the calculation formula of relative bias is $\mathrm{RB} = \left(\overline{\mathrm{X}_{\mathrm{sim}}} - \overline{\mathrm{X}_{\mathrm{obs}}}\right) \Big/ \overline{\mathrm{X}_{\mathrm{obs}}} \times 100\%$ **, where** $\overline{\mathrm{X}_{\mathrm{sim}}}$ **and** $\overline{\mathrm{X}_{\mathrm{obs}}}$ **represent the average value of simulation and observation, respectively. The locations of three rivers (i.e., Yellow River, Yangtze-Huaihe and Yangtze River) are marked by blue lines. The red and green dashed circles represent the whole simulation area and Eastern China, respectively. The purple solid irregular circle indicates mountainous areas, and the red text TJ indicates Tianjin.**
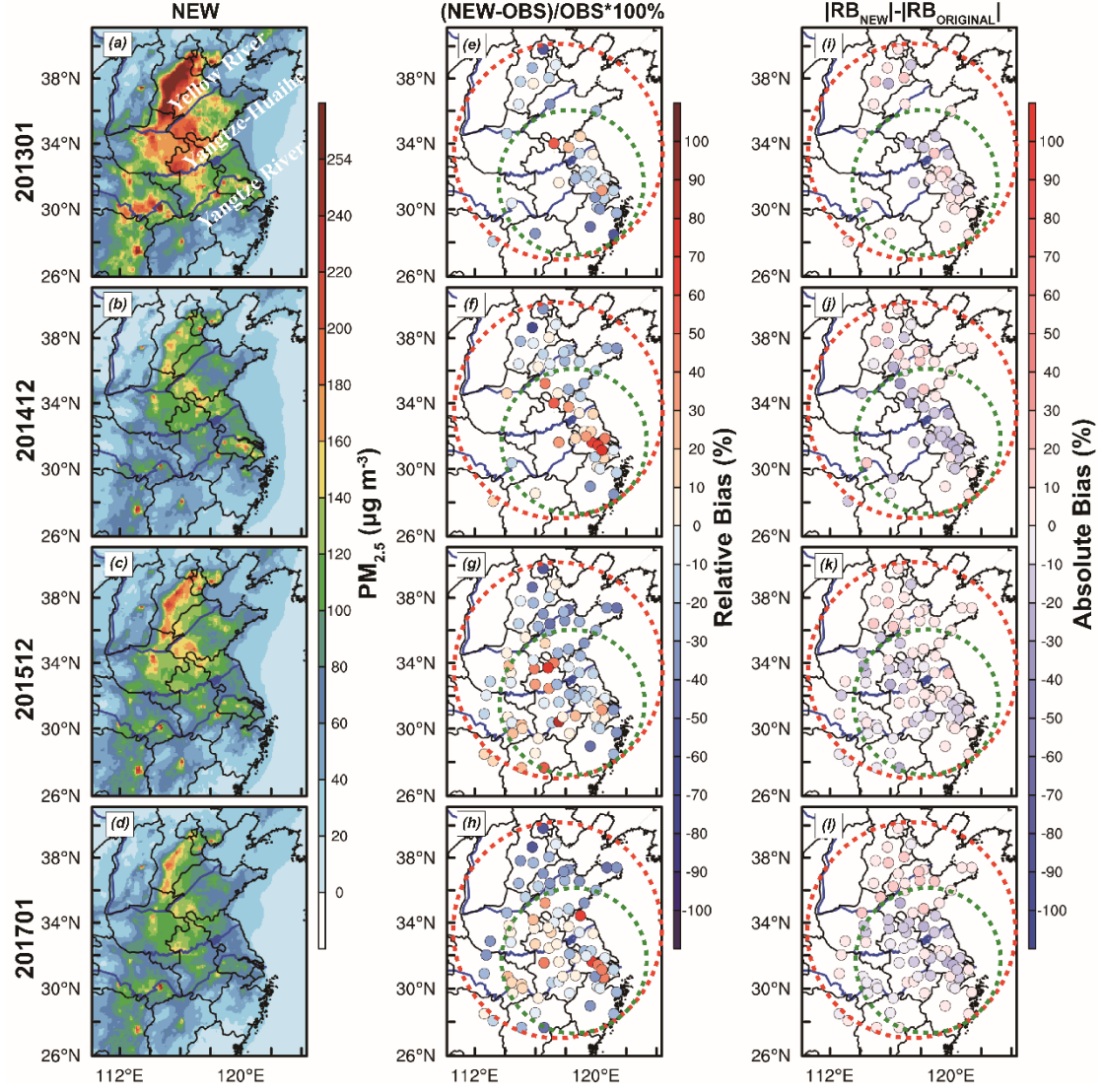
Figure 4. The average value of (a-d) simulated PM$_{2.5}$ concentration (μg m^{-3}) by new schemes, (e-h) the relative bias (RB, %) of PM$_{2.5}$ concentration between simulation of new scheme and observation, (i-l) the absolute bias (AB, %) between new and original schemes, and the calculation formula of absolute bias is $AB = \left| RB_{new} \right| - \left| RB_{original} \right|$, where $\left| RB_{new} \right|$ and $\left| RB_{original} \right|$ represent the relative bias of new and original schemes, respectively. The red and green dashed circles represent the whole simulation area and Eastern China, respectively.
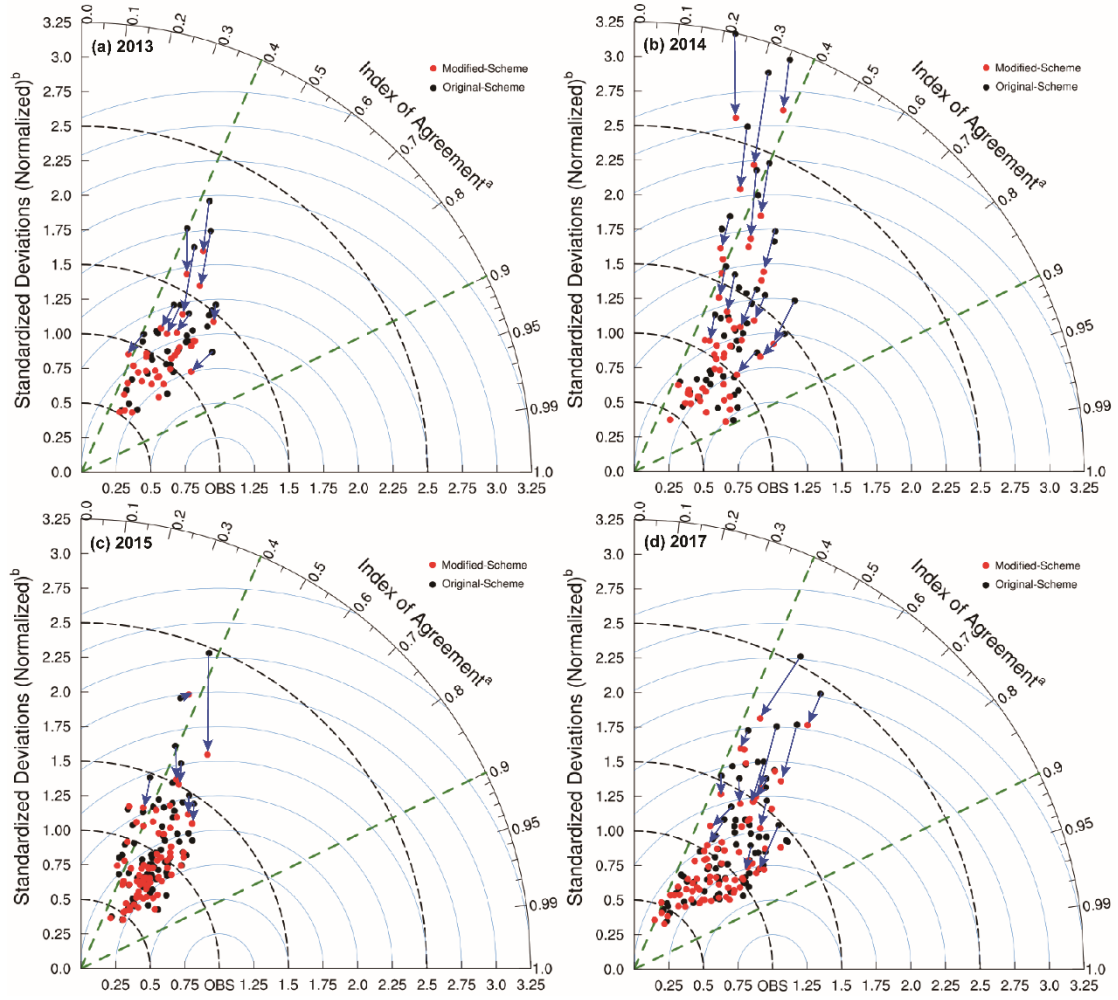
Figure 5. Taylor diagram of simulation by original scheme and modified scheme. XY axes and arc represent the normalized standardized deviations (NSTD,

$$\mathrm{NSTD} = \frac{\sqrt{\dfrac{1}{N-1}\sum_{i=1}^{n}\left(X_{sim,i} - \overline{X_{sim}}\right)^2}}{\sqrt{\dfrac{1}{N-1}\sum_{i=1}^{n}\left(X_{obs,i} - \overline{X_{obs}}\right)^2}} \text{, } \overline{X_{sim}} \text{ and } \overline{X_{obs}} \text{ represent the average value of}$$

710 **simulation and observation, respectively) and index of agreement (IOA,**

$$\mathrm{IOA} = 1 - \frac{\left[\sum_{i=1}^{n} |X_{sim,i} - X_{obs,i}|^2\right]}{\left[\sum_{i=1}^{n} (|X_{sim,i} - \overline{X_{obs}}| + |X_{obs,i} - \overline{X_{obs}}|)^2\right]} \text{, } X_{sim,i} \text{ and } X_{obs,i} \text{ represent the value of}$$

simulated and observed, respectively. i refers to time and n is the total number of time series), respectively. All cities (a total of 35 cities in 2013 and 78 cities in 2014, 2015 and 2017) are shown through dots, and black (red) represents original (new) scheme. The root mean square (RMS) is

715 **denoted by blue dashed line and the arrow indicates the change of the new scheme compared to the original scheme at the same station.**
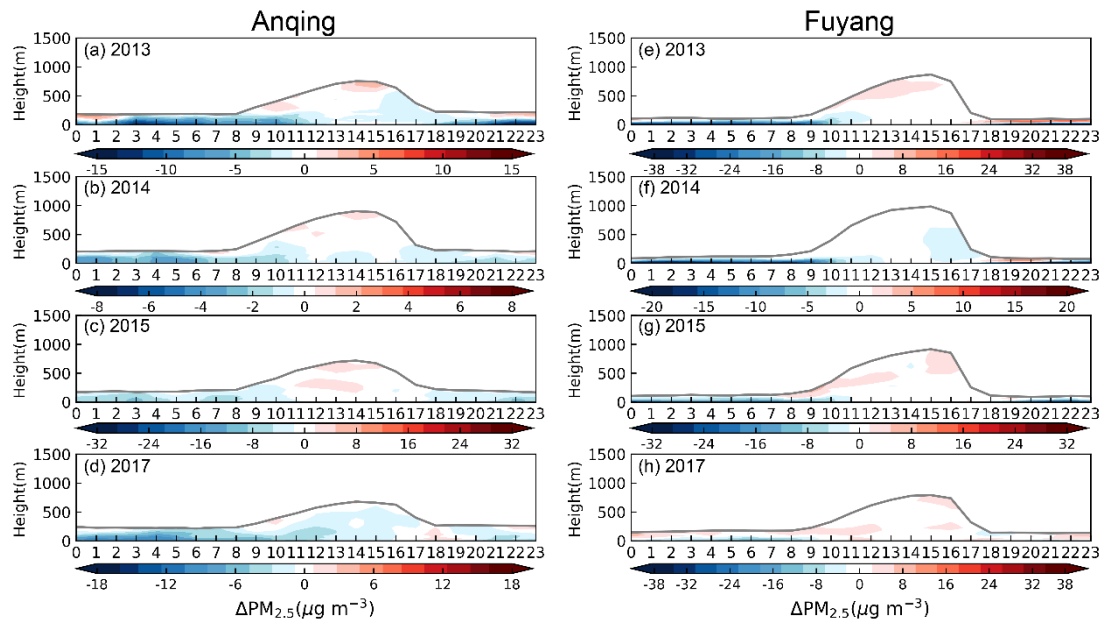
Figure 6. Time-height cross sections for the difference of PM₂.₅ concentration between original and new schemes (i.e., the new scheme minus the original scheme) within the PBL in (a-d) Anqing and (e-h) Fuyang from 2013 to 2017. The gray line indicates the PBLH.
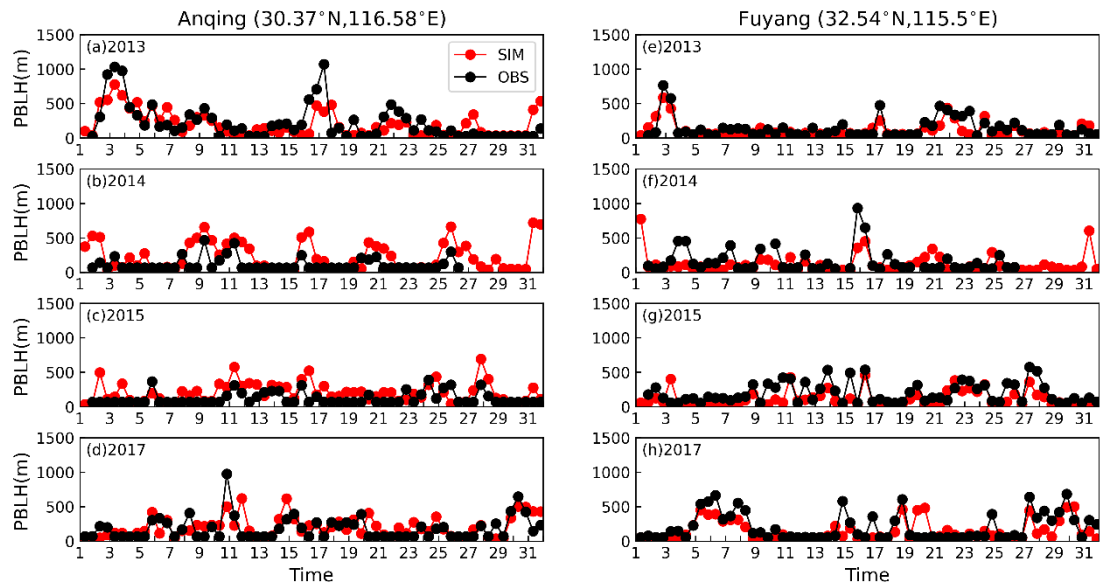
Figure 7. Time series of the observed (black) and simulated (red) PBLH at 0800 and 2000 (BJT) in (a-d) Anqing and (e-h) Fuyang from 2013 to 2017.
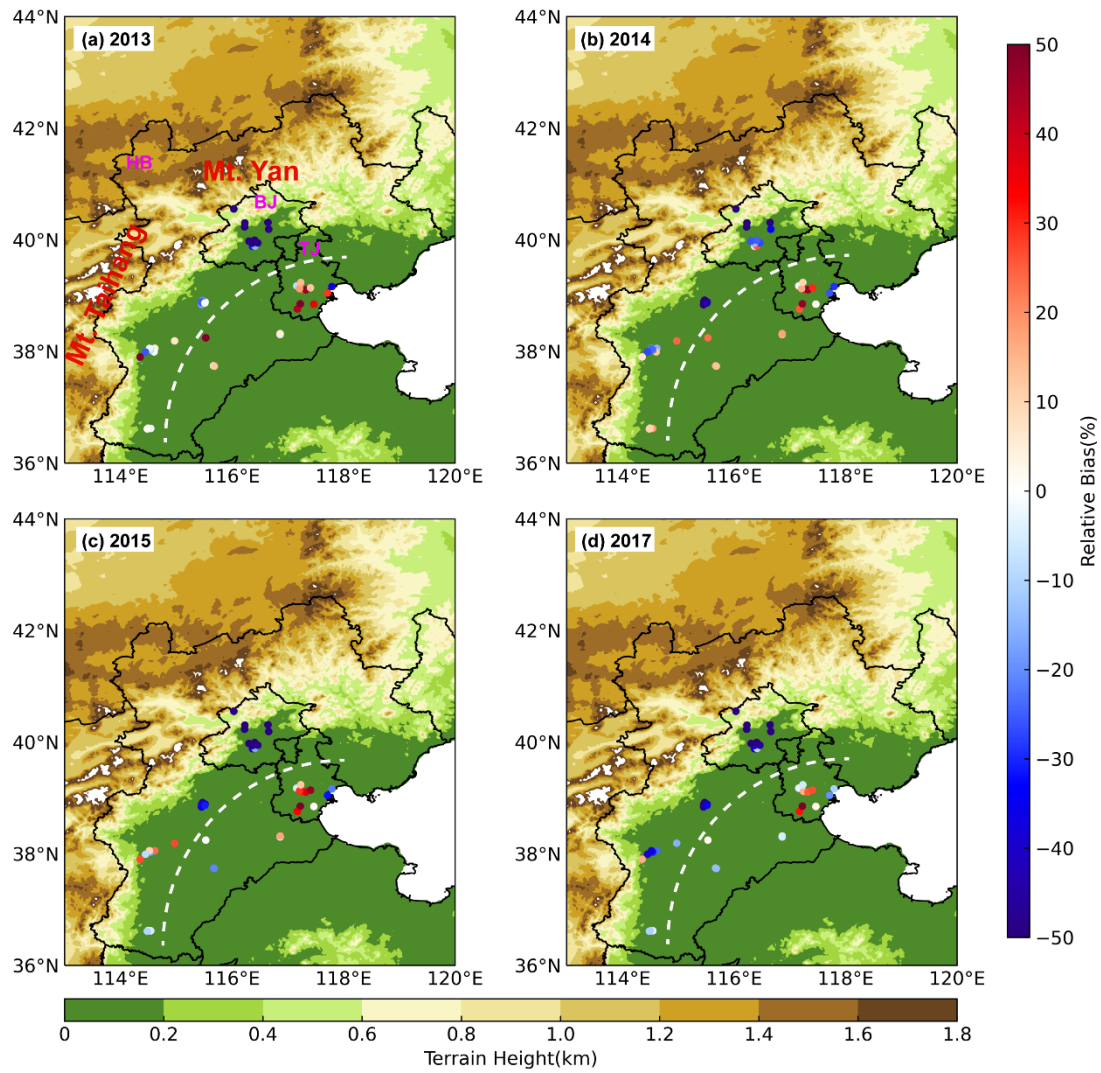
Figure 8. The relative bias (%) between simulation and observation at all environment monitoring stations and terrain height in Beijing-Tianjin-Hebei in (a) 2013, (b) 2014, (c) 2015 and (d) 2017. Taihang Mountain (Mt. Taihang) and Yanshan Mountain (Mt. Yan) are indicated by red text, Beijing (BJ), Tianjin (TJ) and Hebei (HB) are represented by purple abbreviation and the dividing line between overestimated and underestimated areas is indicated by a white dashed line.

730
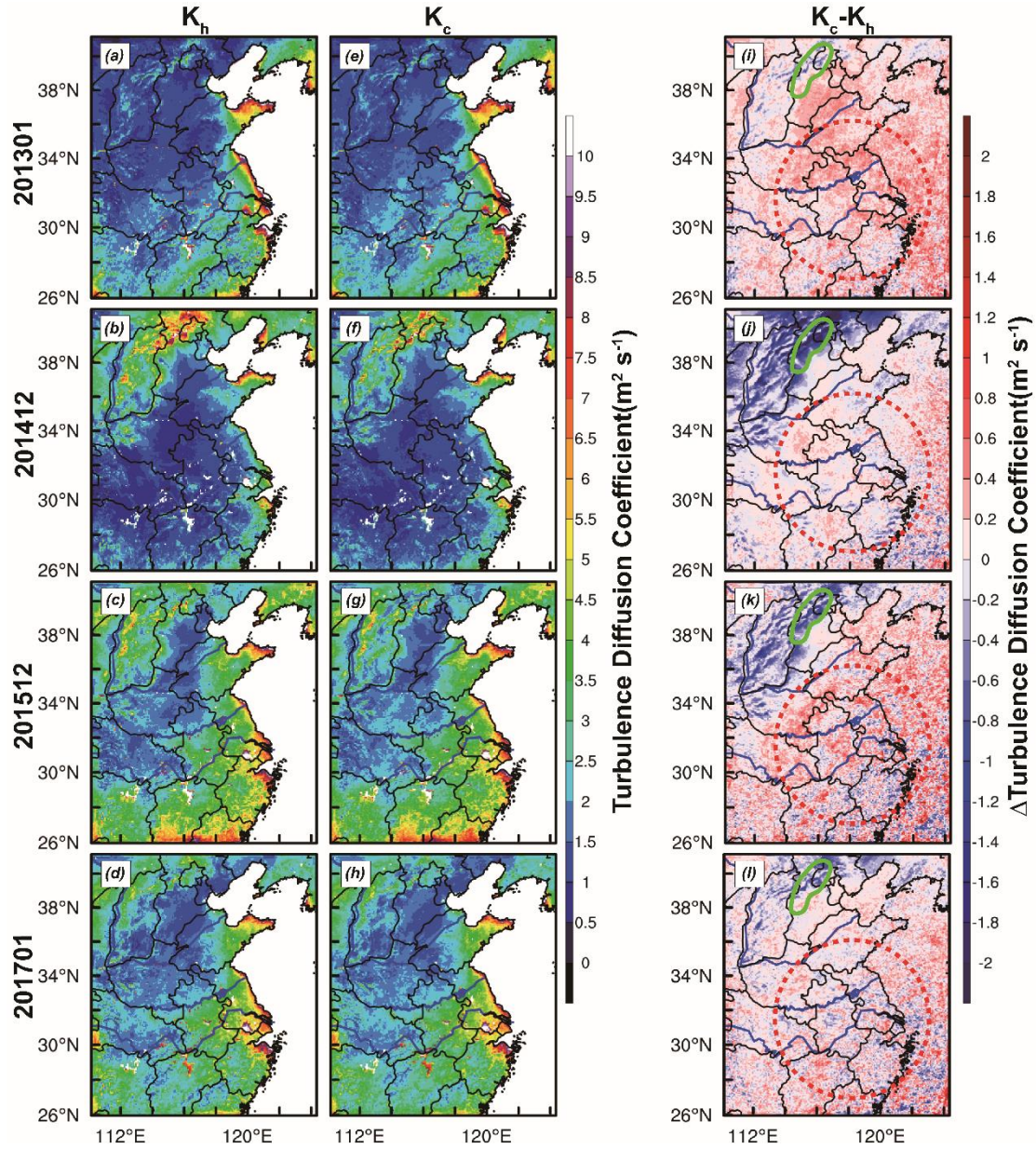
Figure 9. Turbulent diffusion coefficient of (a-d) heat and (e-h) particles, and (i-l) the difference between two turbulent diffusion coefficients. The red dashed and green solid irregular circles represent Eastern China and mountainous areas, respectively.
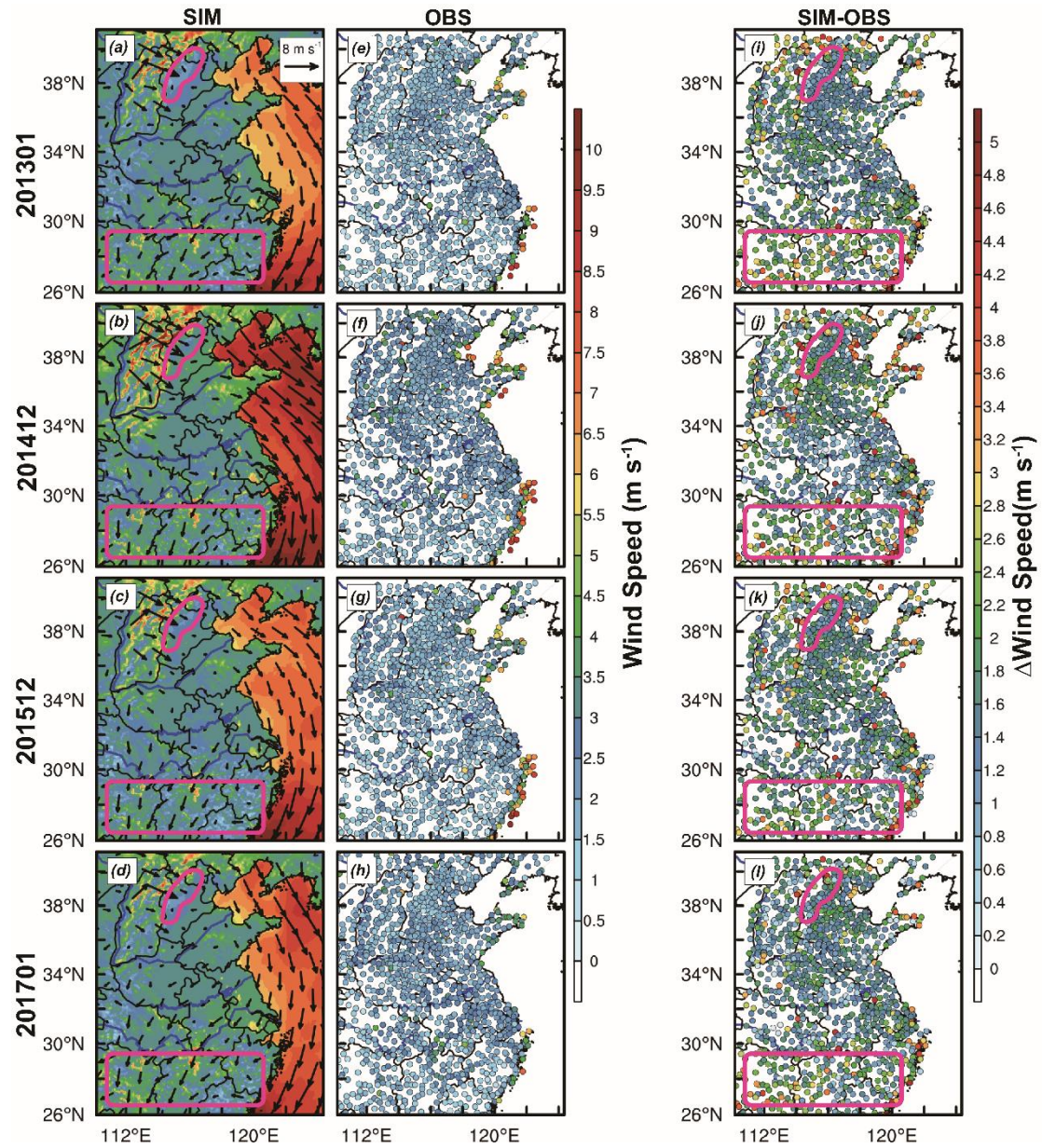
Figure 10. (a-d) Simulated and (e-h) observed wind speed at 10 m above ground level (AGL), and (i-l) the difference of simulated and observed. The purple rectangle indicates the area 740 **where the observed wind speed is significantly overestimated.**